International Journal of Remote Sensing

ISSN: 0143-1161 (Print) 1366-5901 (Online) Journal homepage: https://www.tandfonline.com/loi/tres20

A genetic algorithm solution to the gram-schmidt image fusion

Volkan Yilmaz, Cigdem Serifoglu Yilmaz, Oguz Güngör & Jie Shan

To cite this article: Volkan Yilmaz, Cigdem Serifoglu Yilmaz, Oguz Güngör & Jie Shan (2020) A genetic algorithm solution to the gram-schmidt image fusion, International Journal of Remote Sensing, 41:4, 1458-1485, DOI: 10.1080/01431161.2019.1667553

To link to this article: https://doi.org/10.1080/01431161.2019.1667553

Published online: 22 Sep 2019.

INTERNATIONAL JOURNAL OF REMOTE SENSING
2020, VOL. 41, NO. 4, 1458–1485
https://doi.org/10.1080/01431161.2019.1667553

Taylor & Francis
Taylor & Francis Group

Check for updates

A genetic algorithm solution to the gram-schmidt image fusion

Volkan Yilmaz [a], Cigdem Serifoglu Yilmaz [b], Oguz Güngör [b] and Jie Shan [c]

[a]Department of Geomatics, Artvin Coruh University, Artvin, Turkey; [b]Department of Geomatics, Karadeniz Technical University, Trabzon, Turkey; [c]Lyles School of Civil Engineering, Purdue University, West Lafayette, IN, USA

ABSTRACT

There is no such thing as 'the best image fusion method' in terms of both spectral and spatial fidelity. This fact encourages the researchers to develop more advanced approaches in order to optimally transfer the spatial details without distorting the colour content. Component substitution (CS)-based image fusion methods have been proven to produce sharper images but suffer from colour distortion. The aim of this study was to modify the CS-based Gram-Schmidt (GS) fusion method with the aid of the Genetic Algorithm (GA) to further improve its colour preservation performance. The GA was used to estimate a weight for each multispectral (MS) band. The obtained band weights were used to generate a low-resolution panchromatic (PAN) band, which plays a significant role in the performance of the GS method. The performance of the proposed approach was compared not only against the conventional GS, but also against widely-used CS-based, multiresolution analysis (MRA)-based and colour-based (CB) image fusion methods. The results indicated that the proposed GA-based approach produced spectrally and spatially superior results compared to the other methods used.

ARTICLE HISTORY
Received 19 July 2019
Accepted 4 September 2019

1. Introduction

Today's remote sensing satellites enable the analysts to extract meaningful information from the surface of the earth. Some of these satellites provide more accurate position information, whereas others offer spectrally more enhanced images. However, a wide variety of image processing applications require images with superior spatial and spectral quality. Due to sensor limitations explained by Yilmaz and Gungor (2016a), it may not always be possible to have high-resolution multispectral (MS) or hyperspectral images. Image fusion solves this problem by injecting the spatial details of a higher-resolution panchromatic (PAN) image into a lower-resolution MS or hyperspectral image, producing spatially and spectrally enhanced images. The literature reports a large number of image fusion methods, some of which focus much on retaining the colour quality of the MS image, whereas others on transferring the spatial details at the expense of colour distortion to certain extent. However,

CONTACT Volkan Yilmaz volkanyilmaz.jdz@gmail.com Department of Geomatics, Artvin Coruh University, Artvin, Turkey

image fusion aims at keeping the colour features of the input MS image while sharpening the image.

The image fusion methods can be categorized into three classes as multiresolution analysis (MRA)-based, colour-based (CB) and component substitution (CS)-based methods. The MRA-based methods inject the spatial details extracted from the input PAN band with multiresolution transforms (wavelet, curvelet, contourlet etc.) into the MS bands (Xing et al. 2018). The advantage of the MRA-based methods is that they are successful in preserving the colour content. However, they are not so successful in sharpening the images (Gogineni and Chaturvedi 2018). The CB methods aim to preserve the direction and magnitude of pixel vectors to keep the colour content as much as possible. Performance of these methods are dependent on the statistical relationship between the input images. The CB methods are expected to perform better with single-sensor input images. The CS-based methods transfer the input MS image into a space where the spatial and spectral features can be separated in different components. The input PAN band is replaced by the component with the spatial features. The fused image is produced through an inverse transform (Ghassemian 2016). The CS-based fusion methods produce sharper images but tend to cause a certain amount of colour distortions (Xing et al. 2018; Ghahremani et al. 2019).

Accurate identification of the contributions of the input MS and PAN images to the fusion result plays a significant role in the success of the fusion method used. This, of course, attaches importance on finding a good compromise between the colour and spatial detail quality of the fused images. A comprehensive literature review revealed that, in recent years, the researchers have put so much effort on developing more efficient image fusion approaches to deal with this problem. The recent studies have focused much on developing image fusion approaches based on guided filtering (Li, Kang, and Hu 2013; Yang et al. 2016), multi-scale decomposition (Miao et al. 2011; Dong et al. 2015; Ghahremani and Ghassemian 2015; Chai, Luo, and Zhang 2017; Singh, Garg, and Singh Pannu 2017), hierarchical multimodal probabilistic latent semantic analysis (Fernandez-Beltran et al. 2018), fuzzy logic and gyrator transform (Singh, Kaur, and Singh 2018), spectral embedding and low-rank factorization (Zhang, Wang, and Yang 2016), spectral total variation (Zhao, Lu, and Wang 2017), compressive measurements (Vargas et al. 2018), spectral unmixing (Wei et al. 2016), sparse representation (Yang and Li 2012; Vicinanza et al. 2014; Wang, Jiao, and Yang 2014; Yin 2015; Wei et al. 2015; Chen, Zhang, and Ma 2018; Fei et al. 2019; Yin 2019; Wang et al. 2019; Dian et al. 2019), deep learning (Masi et al. 2016; Wei et al. 2017; Palsson, Sveinsson, and Ulfarsson 2017; Cai et al. 2018; Dian et al. 2018; Scarpa, Vitale, and Cozzolino 2018; Shao and Cai 2018; Yuan et al. 2018; Yang, Zhao, and Chan 2018; Song et al. 2018) and multi-scale decomposition and sparse representation (Cheng et al. 2015).

Another way of finding a balance between the spectral and spatial quality would be using the Genetic Algorithm (GA), which is a nature-inspired metaheuristic optimization technique that is able to search for the optimum solution in very large environments (Holland 1975). Several studies indicated that optimizing the fusion results with GA is a reasonable approach to keep the colour content while sharpening the images. Garzelli and Nencini (2006a) proposed to use GA in the Generalized Intensity-Hue-Saturation (GIHS) method. The authors proposed an injection model that computed the weights used to produce the generalized intensity of the input MS image. The Q4 index (Alparone et al. 2004) was used as the fitness function of the GA. The performance of the proposed method was compared against those of the Ranchin-Wald-Mangolini (Ranchin et al. 2003), à-trous wavelet-based (Garzelli and Nencini 2006b), context-based decision (Aiazzi et al. 2002a), and GIHS methods. The proposed method was found to achieve superior results compared to the other methods. Garzelli and Nencini (2006b) proposed a real-valued GA to maximize the Q4 index in order to achieve the optimum fusion result. They enhanced the performance of the à-trous wavelet transformation method through the use of GA. The proposed method was compared against the Synthetic Variable Ratio (SVR) (Zhang 1999), Spectral Distortion Minimizing (Alparone et al. 2003), Ranchin-Wald-Mangolini (Ranchin et al. 2003), context-based decision (Aiazzi et al. 2002a) and Gram-Schmidt (GS) (Laben and Brower 2000) methods. Masoudi and Kabiri (2014) used a GA-based IHS method for image fusion. The authors first used the GA to estimate a weight for each MS band. The next step was to use a texture-based technique to preserve the colour features in the fused image. The proposed approach was found to be more efficient than the conventional IHS and some of its variants. Lari and Yazdi (2016) proposed an adaptive IHS-based fusion method that employs à-trous wavelet decomposition to extract the high-frequency content from the PAN image. The parameters used in the introduced method were estimated by the GA and Teaching-Learning algorithms. The authors concluded that the presented approach achieved a better performance, compared to the Additive Wavelet Luminance Proportional (Otazu et al. 2005) and Generalized Laplacian Pyramid with Spectral Distortion Minimization (Aiazzi et al. 2002a, 2002b) methods. Niazi, Zade, and Zadeh (2016) also integrated the GAs into the IHS transformation-based fusion method. The used approach was found to outperform the other IHS-based methods in spectral and spatial manner. Khademi and Ghassemian (2017) introduced a multi-objective approach to improve a CS-based fusion method. The authors used the non-dominated sorting GA-II approach to optimize two objective functions, which were the inverse of the Correlation Coefficient (CC) and weighted sum of the Erreur Relative Globale Adimensionalle de Synthese (ERGAS). The proposed method was compared against the other CS-based methods GS, Principal Component Analysis (PCA) and IHS. Quantitative assessment revealed that the proposed approach outperformed the other methods in terms of spectral fidelity. Yilmaz, Serifoglu Yilmaz, and Gungor (2019) improved the performance of the SVR fusion method by using the GA, which was used to estimate the band weights to produce the optimum intensity component. The authors concluded that the presented method produced spectrally and spatially superior results, compared to the other methods used. Despite the fact that image fusion has an extremely extensive literature, the GA has been used in a very small portion of the previous studies.

1.1. Motivation

In order to keep the colour characteristics of the input MS image, it is necessary for the CS-based fusion methods to produce an intensity component that is statistically very similar to the input PAN band. However, there is not a standard procedure to produce the intensity component and the conventional CS-based methods generally consider equal band weights to produce the intensity component. This is actually the main reason for the colour distortion caused by the CS-based methods. The same problem applies for the GS fusion method, one of the most widely used CS-based methods. Since the performance of the GS method depends heavily on the characteristics of the intensity component, researchers have focused on developing some strategies to generate intensity components that enable spatial detail transfer without any colour degradations. An approach was to calculate the intensity component by averaging the MS bands or by a low-pass filter (Laben and Brower 2000). Aiazzi, Baronti, and Selva (2007) used multivariate regression to optimize the intensity component. Garzelli, Nencini, and Capobianco (2008) computed the intensity component by using a weighted average-based approach that considers the mean square error (MSE). Maurer (2013) suggested using the covariance matrix of the MS bands to estimate band weights in order to optimize the intensity component. Pohl and van Genderen (2016) highlighted the challenge in the estimation of the band weights used to generate the intensity component and indicated that the band weights can be estimated by using linear regression, least-square methods or sensors' spectral sensitivity curves. The use of GA, whose potential in optimizing fusion results has been proven in recent studies (Niazi, Zade, and Zadeh 2016; Khademi and Ghassemian 2017; Yilmaz, Serifoglu Yilmaz, and Gungor 2019), would be a reasonable approach to optimize the intensity component used by the CS-based fusion methods. Hence, this study, for the first time in the literature, proposed to utilize the GA to optimize the intensity component used by the CS-based GS method with the aim to increase the colour quality of the GS fusion result. Optimization was done by using the GA to estimate a weight for each input MS band. It should be noted that no previous studies focused on using the GA to optimize the intensity component used by the GS method. This study will contribute to this gap in the literature.

The rest of this paper is organized as follows. Section 2 will introduce the test sites and the data used. Details about the conventional GS method, the proposed GA-based GS method (GA-GS), the other image fusion methods used and the fusion quality evaluation protocols used are also given in Section 2. Section 3 will provide the qualitative and quantitative results and comparisons for the fused images. Section 4 will present the discussion derived from the fusion outcomes. Section 5 will present the conclusions drawn from this study.

2. Material and methodology

2.1. Test sites and data

This study was conducted in three test sites selected in the city of Trabzon. The first site, dominated by buildings, was monitored by the IKONOS satellite, which provides one PAN and four MS bands with spatial resolutions of 1 m and 4 m, respectively. The second site was monitored by the WorldView-2 satellite, which offers one PAN and eight MS bands with spatial resolutions of 50 cm and 2 m, respectively. The second site is a rural area consisting of buildings, trees and other vegetation. The third test site, which is totally a rural area, was monitored by the IKONOS satellite in 2003. The input PAN image of this site was produced by averaging the bands of a 2005 QuickBird pansharpened-image, which had four MS bands with a spatial resolution of 60 cm. Since the input images of this site were acquired by different satellites under different atmospheric conditions, fusion performance in this site was expected to be lower than the other sites. To avoid any land cover inconsistencies due to the 2-year difference between the acquisition dates of the input images of the site 3, this site was selected from the areas on which no land cover changes occurred between 2003 and 2005. The spatial resolution ratio between the input images of this site was greater than those of the other sites, which was another factor that made the fusion process more challenging in this site. The characteristics of the test sites and input images used are summarized in Table 1. The test sites are shown in Figure 1.

2.2. GS image fusion

The GS method, which is a statistical CS-based technique like the PCA, is one of the most widely-used fusion methods. This method de-correlates the input bands utilizing covariance values (Laben and Brower 2000; Pohl and van Genderen 2016). The very first step of the GS method is to simulate a low-resolution PAN (PAN_{sim}) image by using a linear combination of the input MS bands. The conventional GS method simulates the PAN_{sim} image by averaging the MS bands. The GS method considers each band as a high-dimensional vector and combines the PAN_{sim} and MS bands, PAN_{sim} being the first vector. The next step is to apply a GS transformation on the combined data, generating orthogonal vectors. The algorithm applies the projection operator $\mathrm{Proj}_{\boldsymbol{a}}$ for the vectors $\boldsymbol{a}$ and $\boldsymbol{b}$ as;

$$\mathrm{Proj}_{a}(\boldsymbol{b}) = \frac{\langle \boldsymbol{a}|\boldsymbol{b}\rangle}{\langle \boldsymbol{a}|\boldsymbol{a}\rangle}\boldsymbol{a} \tag{1}$$

where, $\boldsymbol{a}|\boldsymbol{b}$ is the inner product of $\boldsymbol{a}$ and $\boldsymbol{b}$. The result of this operator is the projection of the vector $\boldsymbol{b}$ onto the line spanned by vector $\boldsymbol{a}$ (Pohl and van Genderen 2016). The GS method produces the orthogonal vectors with the following equations;

$$\begin{aligned} \boldsymbol{a}_1 &= \boldsymbol{b}_1 \\ \boldsymbol{a}_2 &= \boldsymbol{b}_2 - \mathrm{Proj}_{\boldsymbol{a}_1}(\boldsymbol{b}_2) \\ \boldsymbol{a}_3 &= \boldsymbol{b}_3 - \mathrm{Proj}_{\boldsymbol{a}_1}(\boldsymbol{b}_3) - \mathrm{Proj}_{\boldsymbol{a}_2}(\boldsymbol{b}_3) \end{aligned} \tag{2}$$

where, $m = n + 1$ (total number of MS bands plus panchromatic band), and $\boldsymbol{a}_1, \boldsymbol{a}_2 \ldots \boldsymbol{a}_m$ are normalized orthogonal vectors that are then ortho-normalized ($\boldsymbol{c}_1, \boldsymbol{c}_2 \ldots \boldsymbol{c}_m$) as (Pohl and van Genderen 2016);

$$\boldsymbol{c}_m = \frac{\boldsymbol{a}_m}{||\boldsymbol{a}_m||} \tag{3}$$

After forward GS transformation, the histogram-matched PAN band is replaced by the first GS component. It should be noted that all MS bands are resampled to the size of

Table 1. Characteristics of the test sites and input images used.

		Input MS data		Input PAN data	
Site	Type	Imagery	Year	Imagery	Year
1	Urban	IKONOS MS	2003	IKONOS PAN	2003
2	Urban+Rural	WorldView-2 MS	2012	WorldView-2 PAN	2012
3	Rural	IKONOS MS	2003	QuickBird pansharpened	2005

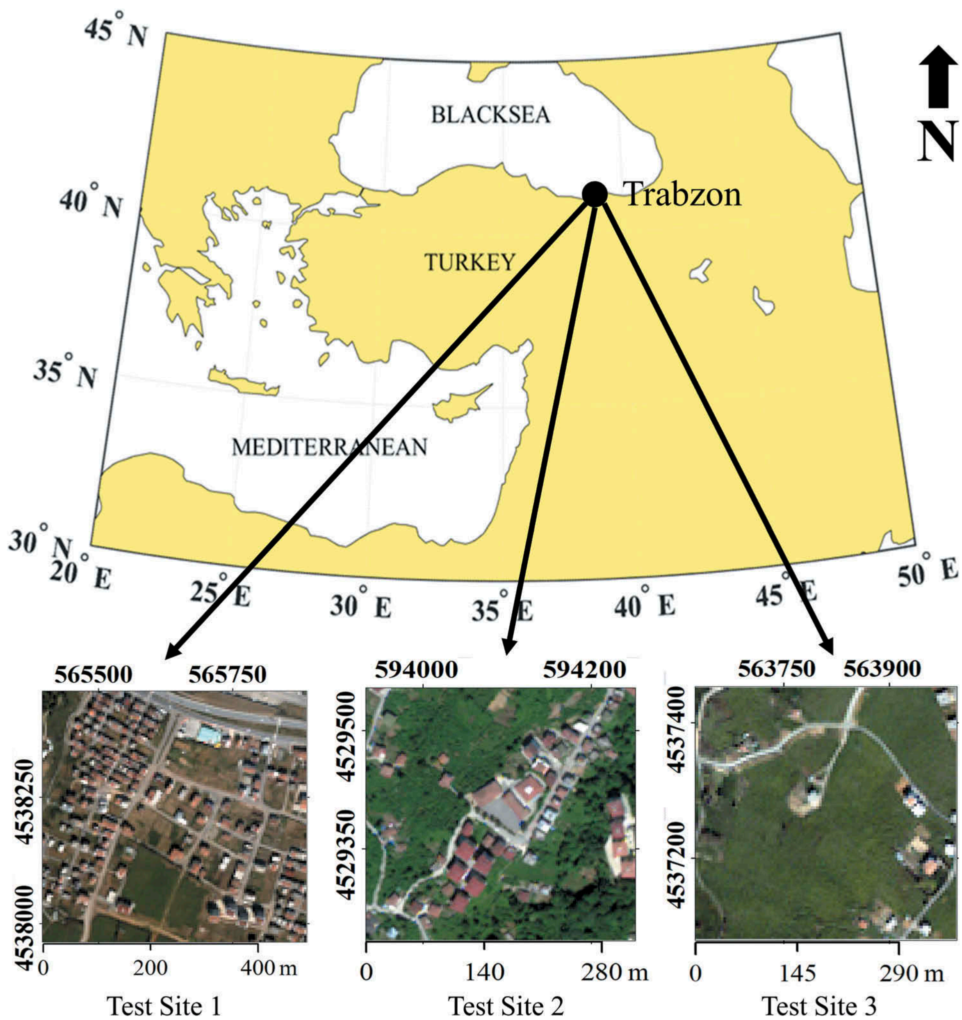

Figure 1. Test sites.

the PAN image. As a final step, an inverse GS transformation is applied to obtain the fused image (Laben and Brower 2000; Pohl and van Genderen 2016).

2.3. The proposed GA-based GS method

This study proposed to utilize the GA to estimate the band weights used to optimize the PAN_{sim} images. The GA is a metaheuristic randomized search and optimization method based on the principles of natural genetics and evolution (Holland 1975; Maulik and Bandyopadhyay 2000). It has been proven to provide a robust search in complex environments (Yu 1998) by implementing a 'survival of the fittest' strategy. Compared to conventional optimization techniques, GAs require less prior information about the problem to be solved (Hole, Gulhane, and Shellokar 2013), which is a huge advantage especially when dealing with a large data set.

2.3.1. Population initialization

The very first step of a GA is to produce a population, which comprises of randomly generated chromosomes. Each chromosome in turn consists of randomly-generated genes, which are the candidate band weights used to produce the intensity component. The diversity of the population should be maintained in order not to end up with a condition known as 'premature convergence', which means the convergence of the algorithm before the global optimum solution is achieved. If this condition occurs, the parental solutions cannot produce offsprings that are superior to their parents. In order to ensure the diversity of the population, for all test sites, we generated populations consisting of 1000 chromosomes, each consisting of genes between 0 and 1. Since the input MS images of the sites 1, 2 and 3 have 4, 8 and 4 MS bands, respectively, the length of each chromosome was 4, 8 and 4 in the sites 1, 2 and 3, correspondingly.

2.3.2. Fitness evaluation

The fitness function evaluates the closeness between a candidate solution (i.e. chromosome) and the optimum solution, i.e. it determines how fit a solution is. The fitness function should be able to quantitatively measure the fitness of a candidate solution. Hence, in this study, we used the Root Mean Square Error (RMSE) function to evaluate the fitness of each chromosome since it has been used in many previous studies to evaluate the spectral fidelity of the fused images. The RMSE is given as;

$$\mathrm{RMSE} = \sqrt{\frac{1}{p}\sum_{i=1}^{p}\left(\mathbf{MS}(k)_i - \mathbf{F}(k)_i\right)^2} \tag{4}$$

where, $\mathbf{MS}(k)$ and $\mathbf{F}(k)$ denote the k^{th} MS and fused bands, respectively. p denotes the total number of pixels.

The objective function of a GA is the function to be optimized. In GA, each candidate solution is used in the objective function to determine a fitness value for each chromosome. This value is used to select the chromosomes that produce fitter chromosomes. The proposed GA-GS method aims to improve the performance of the conventional GS method, which computes the intensity (**I**) component by averaging all input MS bands. The proposed method uses the GA to estimate a weight for each MS band to optimize the **I** component, which is calculated as the weighted average of the MS bands. The objective function of the GA is given in Equation (5).

$$\mathbf{I} = \frac{1}{\sum w_i}\sum_{i=1}^{n} w_i \times \mathbf{MS}_i \tag{5}$$

where, **I** is the intensity component, $\mathbf{MS}_i$ is the i^{th} band of the input MS image and w_i is the weight of i^{th} band.

2.3.3. Selection

The GAs select a small portion of the chromosomes from the population for further evolution. A proper chromosome selection procedure should consider two factors. First, fitter chromosomes should have better chances to survive, whilst the weaker ones perish. This factor facilitates the convergence in the evolution. The other factor is that the selection should be in a random way. A smaller search space is explored if a less random selection procedure is applied (Qiu et al. 2015). Hence, in this study, the roulette wheel selection procedure (Shukla, Pandey, and Mehrotra 2015), which is one of the most widely-used chromosome selection techniques, was used to select the chromosomes to be used to produce fitter chromosomes. The roulette wheel selection considers a wheel that is divided into s pies, s being the number of the chromosomes in the population. Each chromosome gets a portion of the circle that is proportional to its fitness value. A fixed point is then selected on the wheel. The wheel is rotated, and the region that corresponds to the fixed point is chosen as a parent. The same process is repeated to obtain the second parent. The selected chromosomes survive to the next generation and are used to produce new offsprings with crossover and mutation operations (Tang et al. 1996).

2.3.4. Crossover

The crossover operator exchanges information between two parent chromosomes. The aim of this operator is to search the close neighbourhood around the parent to produce the offspring. At least one crossover point is chosen on chromosomes. The string from the beginning of a chromosome to the crossover point is copied from a parent and the rest is copied from another parent. Lam et al. (2004) indicated that a crossover rate between 60% and 95% is efficient. A number of trial-and-error procedures were conducted to find the optimum crossover rates. Chromosomes obtained from the crossover operation is replaced by the old ones. It is not possible to obtain the optimum solution just by searching the neighbourhood, if the algorithm is trapped at a local minimum. Because, crossover operator searches the neighbourhood in very small steps instead of big leaps, leading to the same local minimum values again. In such cases, the diversity of the population should be increased with the mutation operation to avoid this problem.

2.3.5. Mutation

In cases where the offsprings produced by the crossover operator resemble to their parents, the diversity of the population is increased with the mutation operator to prevent the premature convergence. The mutation operator randomly changes some part of the chromosomes. Lam et al. (2004) indicated that the mutation rate should be low, at about 0.5-1%. The chromosomes subject to mutation is replaced by the old ones.

2.3.6. Termination

The selection, crossover and mutation operators continue to iterate until the population is converged. In other words, the algorithm terminates when the offsprings that are not significantly different from the previous ones are produced. A maximum iteration number is also set in case the algorithm does not converge. The GA-GS method is implemented in MATLAB environment. The flowchart of the proposed approach is given in Figure 2.

2.4. Image fusion methods used

This subsection provides the theories of the image fusion methods that were compared against the proposed fusion method. The Wavelet Single Band (WSB) method is one of

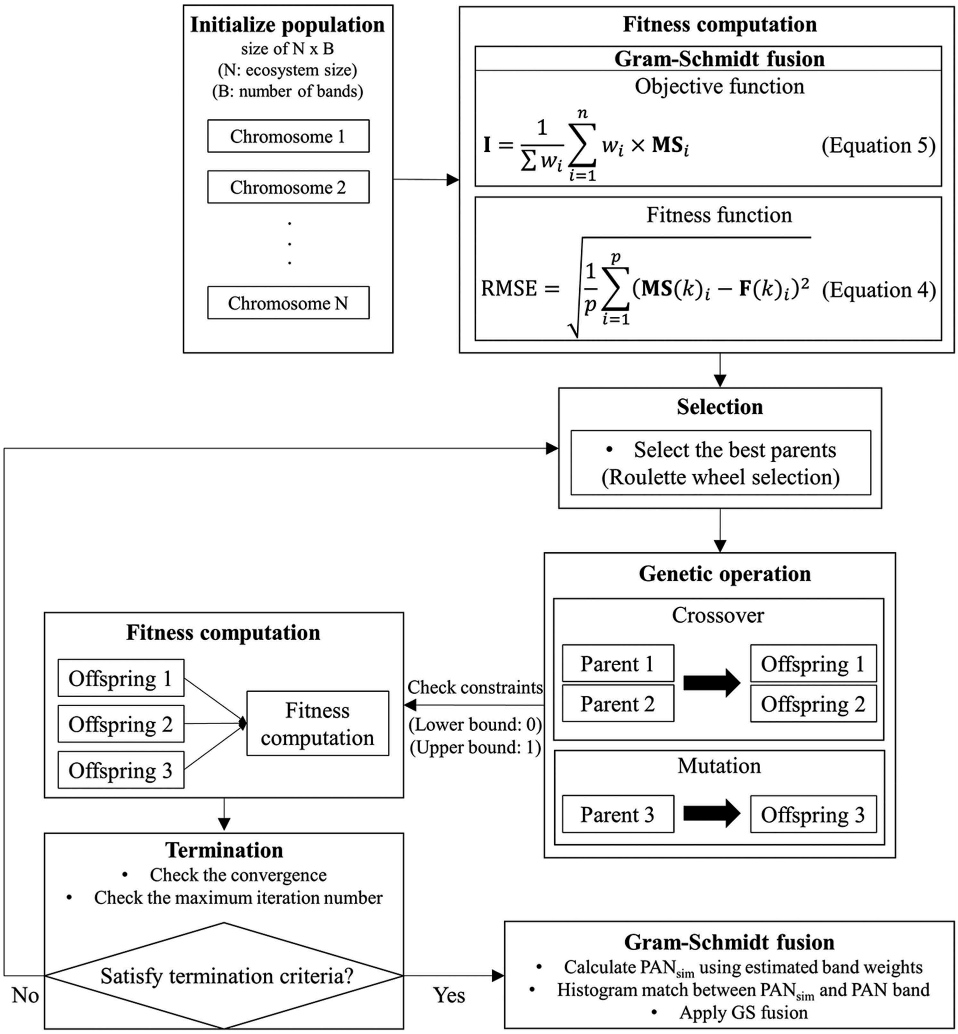

Figure 2. Flowchart of the proposed approach.

the most popular MRA-based fusion methods. This method applies successive 2D Discrete Wavelet Transformations (DWT) on the input PAN image. The number of transformations is dependent on the spatial resolution ratio between the input images. Then, each MS band is replaced by the approximation image obtained from the DWT. The fused image is produced through an inverse DWT (Hill, Canagarajah, and Bull 2002; Yilmaz and Gungor 2016a).

The CB methods considered in this study were the High-Pass Filtering (HPF) and Smoothing Filter-based Intensity Modulation (SFIM). The HPF method enhances the spatial details of a PAN image with a high-pass filter and injects these details into an MS image (Schowengerdt 1980). The SFIM method is based on simplified land surface reflection and solar radiation model. This method aims at transferring the spatial details using a ratio computed between a PAN image and a lower resolution smoothed image (Liu 2000; Wald and Ranchin 2002; Snehmani et al. 2017).

The conventional CS-based methods used in this study include the Multiplicative (MCV), Brovey (BRV), GIHS, PCA, Hyperspherical Colour Space (HCS) and GS. The MCV method performs in a very simple manner. It produces fused images by multiplying each MS band by the PAN band (Crippen 1989). The BRV method, another simple fusion method based on arithmetic operations, produces fused images by multiplying each MS band by the PAN band and dividing the result by the intensity component obtained by summing the input MS bands (Hallada and Cox 1983). The GIHS method is a generalized version of the conventional IHS transformation-based fusion technique where an IHS transformation is applied on the original RGB image to generate the intensity, hue and saturation components (Siddiqui 2003). After replacing the intensity component by the PAN band, an inverse IHS transformation is performed to produce the fused image. The GIHS method can handle more than three MS bands, in contrast to the conventional IHS-based method (Siddiqui 2003). The PCA method applies a PCA transformation on the input MS image (Chavez and Kwarteng 1989). The first principal component is substituted by the PAN band, assuming that both input images are identical except for their spatial resolutions (Yilmaz and Gungor 2016a). The last step is to apply an inverse PCA transformation on this new image to obtain the fused image. The HCS method generates a smoothed PAN image as the first step. Afterwards, the imagery is transformed from native colour space to hyperspherical colour space. The algorithm then matches the intensity of the MS image to those of the squares of the original and smoothed PAN images. The squares of the smoothed PAN, original PAN and MS intensity are used to form an adjusted intensity. Fused image is produced through an inverse transformation (Padwick et al. 2010).

2.5. Fusion quality evaluation

This study evaluated the spectral fidelity of all fused images by using the metrics RMSE, ERGAS (Wald 2002), Feature Similarity (FSIM) (Zhang et al. 2011), Universal Image Quality Index (UIQI) (Wang and Bovik 2002), Visual Information Fidelity for Fusion (VIFF) (Han et al. 2013), Feature Mutual Information (FMI) (Haghighat, Aghagolzadeh, and Seyedarabi 2011), Gradient Similarity (GSM) (Liu, Lin, and Narwaria 2012) and Structural Similarity (SSIM) (Wang and Li 2011). The spatial detail quality of the fused images was evaluated by calculating the CC between the fused bands and input PAN band. The best value for the RMSE and ERGAS is 0; whereas 1 for the others. The mathematical expressions of all these metrics are given in Table 2.

This study used Wald's first property (Wald, Ranchin, and Mangolini 1997) to evaluate the fusion results. According to this property, a fused image that is downsampled to the size of the input MS image is as identical as possible to the input MS image. Hence, the RMSE, ERGAS, FSIM, UIQI, VIFF, FMI, GSM and SSIM spectral quality metrics were computed between the input MS images and downsampled fused images. Downsampling was applied by using the nearest neighbour technique to keep the colour content as much as possible. This strategy was also used by Park and Kang (2004), Padwick et al. (2010) and Yilmaz and Gungor (2016a). The CCs were calculated both between the input MS and PAN images and between fused and PAN images in

Table 2. Mathematical expressions of the spectral and spatial quality metrics used.

Metric	Mathematical model
RMSE (spectral)	See Equation (4)
ERGAS (spectral)	$$\mathrm{ERGAS} = 100\frac{h}{l}\sqrt{\frac{1}{K}\sum_{k=1}^{K}\left(\frac{\mathrm{RMSE}(k)}{\mu(k)}\right)^2}$$ where, h and l are the spatial resolutions of the input PAN and MS image, respectively. $\mu(k)$ is the mean of the k^{th} band and K is the total number of bands.
FSIM (spectral)	$$\mathrm{FSIM} = \frac{\sum_{x\in\Omega} S_L(x)\cdot PC_m(x)}{\sum_{x\in\Omega} PC_m(x)}$$ Let α and β be the parameters used to adjust the relative importance of the PC and G, which are the components used to calculate the similarity. S_L is calculated as; $$S_L(x) = [S_{PC}(x)]^{\alpha}\cdot[S_G(x)]^{\beta},$$ where, $$S_{PC}(x) = \frac{2PC_1(x)\cdot PC_2(x)+T_1}{PC_1^2(x)+PC_2^2(x)+T_1} \qquad S_G(x) = \frac{2G_1(x)\cdot G_2(x)+T_2}{G_1^2(x)+G_2^2(x)+T_2}$$
UIQI (spectral)	$$\mathrm{UIQI} = \frac{4\sigma_{xy}\bar{\mathbf{x}}\bar{\mathbf{y}}}{(\bar{\mathbf{x}}^2+\bar{\mathbf{y}}^2)\left(\sigma_x^2+\sigma_y^2\right)}$$ where, $\mathbf{x} = \{\mathbf{x}_1, \ldots, \mathbf{x}_n\}$ and $\mathbf{y} = \{\mathbf{y}_1, \ldots, \mathbf{y}_n\}$ show the original MS and fused images, respectively. $\bar{\mathbf{x}}$ is the mean of the original MS band, $\bar{\mathbf{y}}$ is the mean of the corresponding fused band, σ_x^2 is the variance of $\mathbf{x}$, σ_y^2 is the variance of $\mathbf{y}$ and σ_{xy} is the covariance between $\mathbf{x}$ and $\mathbf{y}$.
VIFF (spectral)	$$\mathrm{VIFF}_k(\mathrm{I}_1, \ldots, \mathrm{I}_n, \mathrm{I}_F) = \frac{\sum_b \mathrm{FVID}_{k,b}(\mathrm{I}_1, \ldots, \mathrm{I}_n, \mathrm{I}_F)}{\sum_b \mathrm{FVIND}_{k,b}(\mathrm{I}_1, \ldots, \mathrm{I}_n, \mathrm{I}_F)}$$ where, $$\mathrm{FVIND}_{k,b}(\mathrm{I}_1, \ldots, \mathrm{I}_n, \mathrm{I}_F) = \mathrm{VIND}_{k,b}(\mathrm{I}_t, \mathrm{I}_F) \qquad \mathrm{VIND}_{k,b}(\mathrm{I}_i, \mathrm{I}_F) = \frac{1}{2}\log_2\left(\frac{\left\|s_{k,b}^2 C_U+\sigma_N^2\mathrm{I}\right\|}{\left\|\sigma_N^2\mathrm{I}\right\|}\right)$$
FMI (spectral)	$$\mathrm{FMI}_F^{AB} = \frac{I_{FA}}{H_F+H_A}+\frac{I_{FB}}{H_F+H_B}$$ where, H_A, H_B and H_F stand for the histogram-based entropies of the MS image (A), PAN image (B) and fused image (F). I_{FA} and I_{FB} denote the amount of information.
GSM (spectral)	$$\mathrm{GSM} = \frac{2g_x g_y+C_4}{g_x^2+g_y^2+C_4}$$ where, g_x and g_y stand for the gradient values for the original MS and fused image, respectively. C_4 is a small constant.
SSIM (spectral)	$$\mathrm{SSIM}(\mathbf{x},\mathbf{y}) = \frac{\left(2\mu_x\mu_y+C_1\right)\left(2\sigma_{xy}+C_2\right)}{\left(\mu_x^2+\mu_y^2+C_1\right)\left(\sigma_x^2+\sigma_y^2+C_2\right)}$$ where, μ_x, μ_y, σ_x^2, σ_y^2 and σ_{xy} stand for the mean of the original MS image, mean of the fused image, variance of the original MS image, variance of the fused image and covariance between the original MS and fused image, respectively. C_1 and C_2 are computed as $C_1 = (K_1L)^2$ and $C_2 = (K_2L)^2$.
CC (spatial)	$$\mathrm{CC} = \frac{\sum_m\sum_n\left(\mathrm{PAN}_{mn}-\overline{\mathrm{PAN}}\right)\left(\mathrm{F}_{mn}-\bar{\mathrm{F}}\right)}{\sqrt{\sum_m\sum_n\left(\mathrm{PAN}_{mn}-\overline{\mathrm{PAN}}\right)^2\left(\mathrm{F}_{mn}-\bar{\mathrm{F}}\right)^2}}$$ where, $\bar{\mathrm{F}}$ and $\overline{\mathrm{PAN}}$ are the mean of the fused images and PAN band, respectively.

Table 3. Full forms of the abbreviations used.

Abbreviation	Full form
BRV	Brovey
CB	Colour-based
CC	Correlation coefficient
CS	Component substitution
DWT	Discrete Wavelet Transformation
ERGAS	Erreur Relative Globale Adimensionalle de Synthese
FMI	Feature Mutual Information
FSIM	Feature Similarity
GA	Genetic Algorithm
GIHS	Generalized Intensity-Hue-Saturation
GS	Gram-Schmidt
GSM	Gradient Similarity
HCS	Hyperspherical Colour Space
HPF	High-Pass Filtering
IHS	Intensity-Hue-Saturation
MCV	Multiplicative
MRA	Multiresolution analysis
MS	Multispectral
PAN	Panchromatic
PCA	Principal Component Analysis
SFIM	Smoothing Filter-based Intensity Modulation
SSIM	Structural Similarity
SVR	Synthetic Variable Ratio
UIQI	Universal Image Quality Index
VIFF	Visual Information Fidelity for Fusion
WSB	Wavelet Single Band

order to investigate whether or not the used fusion methods were successful in transferring the spatial details. The fusion methods that resulted in the greater CC increase were considered more successful in spatial regard. In order to ensure a fair comparison among the fusion methods used, each method was given a score between 1 to 10 with respect to its success in spectral and spatial regard. This approach was also used by Yilmaz and Gungor (2016a, 2016b) and Yilmaz, Serifoglu Yilmaz, and Gungor (2019). Full forms of the abbreviations used in this study are given in Table 3.

3. Results and evaluations

In this study, the performance of the proposed GA-GS approach was compared not only against that of the conventional GS, but also against those of the MCV, BRV, GIHS, PCA, HPF, HCS, SFIM and WSB methods qualitatively and quantitatively. This section presents the qualitative and quantitative evaluation results.

3.1. Qualitative evaluation

A successful image fusion method enables the transferring of spatial details without deteriorating the colour characteristics of the input MS image. Hence, it is reasonable to assess the colour quality of a fused image by visually comparing it against the input MS image. Figure 3 shows the input images and fusion results of the site 1. The figure also shows subsamples from the fusion results for further investigation. To ensure a fair comparison, all subfigures given in Figure 3 are shown in true colour band combination without any contrast stretch procedure applied. As seen from Figure 3(a), the MCV, BRV, GIHS, HCS and GS methods deteriorated the

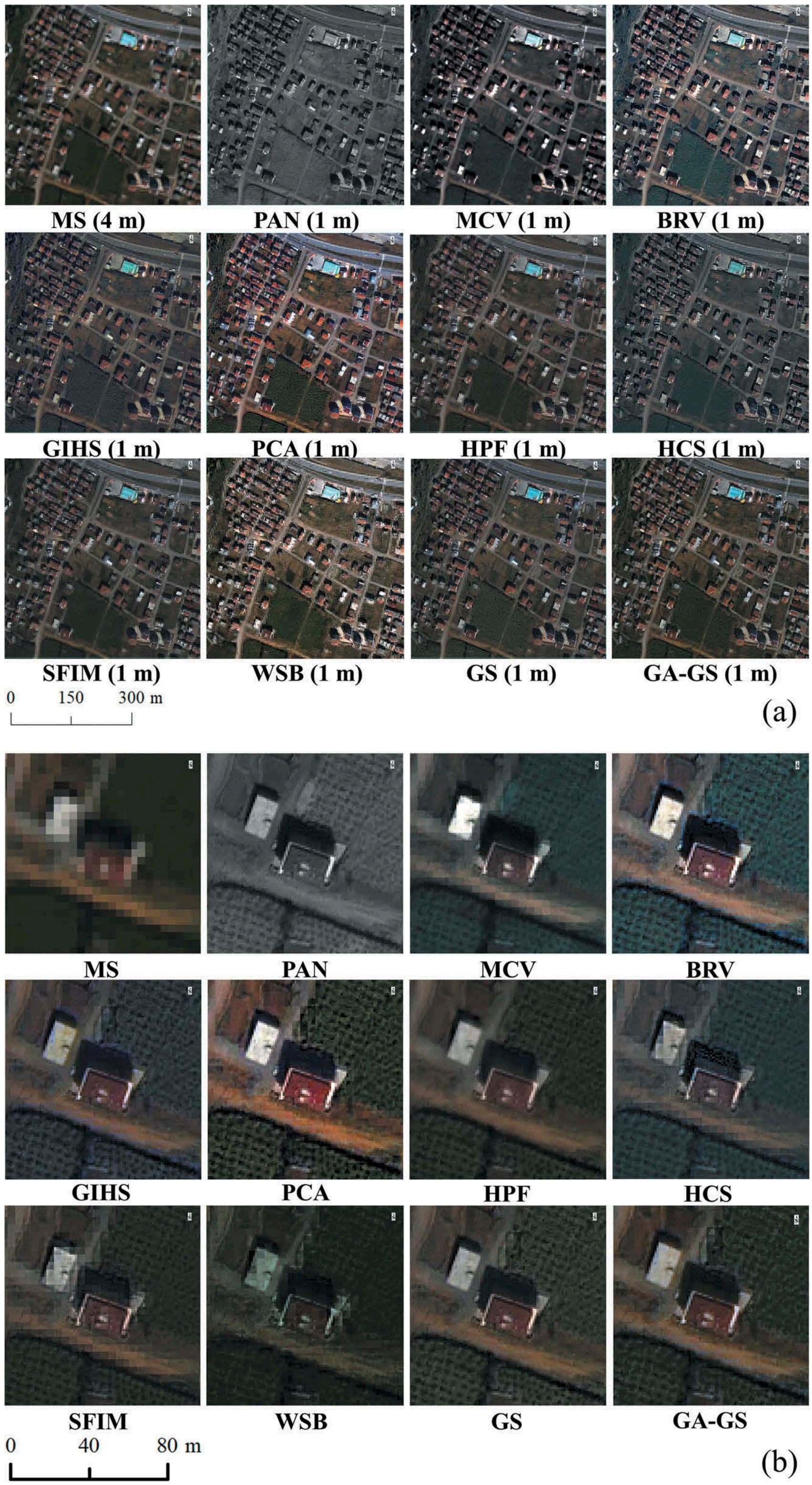

Figure 3. (a) Fused images for the site 1, (b) subsamples from (a).

global colour content of the input MS image of the site 1, whereas the PCA, HPF and SFIM methods caused less amount of colour distortions. Figure 3(a) also shows that the WSB and GA-GS methods kept the global colour content better than the others. On the other hand, the WSB, HPF and SFIM methods were found to produce images with low spatial fidelity in the site 1, which can be seen in Figure 3(b). The MCV, BRV, GIHS, PCA, GS and GA-GS methods produced sharper images in the site 1.

Figure 4 presents the input images and fusion results of the site 2. The figure also shows a smaller portion of the fused images for further assessment. All subfigures presented in Figure 4 are displayed in true colour band combination without any contrast stretch procedure. As seen from Figure 4(a), in the site 2, the MCV, BRV, GIHS, WSB and PCA methods produced images whose global colour contents were not consistent with that of the input MS image. These methods caused significant colour distortions on the roofs, shadows and vegetation, which can also be seen in Figure 4(a). On the other hand, the HPF, HCS, SFIM, GS and GA-GS methods produced spectrally more consistent images in general. However, the SFIM and WSB methods caused some colour distortions especially in the areas where frequency changed. Figure 4(b) shows that all methods except the PCA and WSB produced sharper images. Pixelated effects are apparent on the results of the PCA and WSB results in the site 2.

Figure 5 demonstrates the input images and fusion results of the site 3. Subsamples from the fusion results of this site are also shown in Figure 5. Note that all subfigures in this figure are displayed in true colour band combination without any contrast stretch. Figure 5(a) shows that the GA-GS method achieved visually the best colour quality, whereas the HPF, GS and SFIM methods can be said to be the other successful ones in this regard. The SFIM method caused some colour artefacts in shadowy areas in the site 3, which can also be observed in Figure 5(a). As also seen in Figure 5(a), the BRV, HCS and GIHS methods preserved the global colour characteristics to a certain extent. On the other hand, the MCV, PCA, GIHS and WSB methods produced inconsistent colours in the site 3. The GA-GS, BRV, HCS, SFIM, GIHS and HPF methods produced the sharpest images in this site (see Figure 5(b)), whereas the WSB and PCA methods failed to transfer the spatial details.

In spite of the fact that qualitative evaluation presents a general view on the performances of the fusion methods used, it is highly subjective and depends heavily on analyst's point of view and monitor specifications. Hence, quantitative evaluation is needed for a more reasonable investigation.

3.2. Quantitative evaluation

3.2.1. Spectral quality evaluation

Table 4 shows the spectral metric values calculated from the fused images of the test sites. As seen from the table, the proposed GA-GS approach resulted in the best RMSE, ERGAS, FSIM, UIQI, GSM and SSIM values in the site 1. The best VIFF and FMI values were achieved by the MCV method in the site 1. Table 4 also reveals that the WSB method got the second best metric values after the GA-GS approach in the site 1, which is in compliance with visual findings. As also seen from Table 4, the PCA method was found to yield promising results in terms of spectral fidelity. The fused images produced by the HCS, MCV, GIHS and BRV methods got the worst metric values in the site 1, which

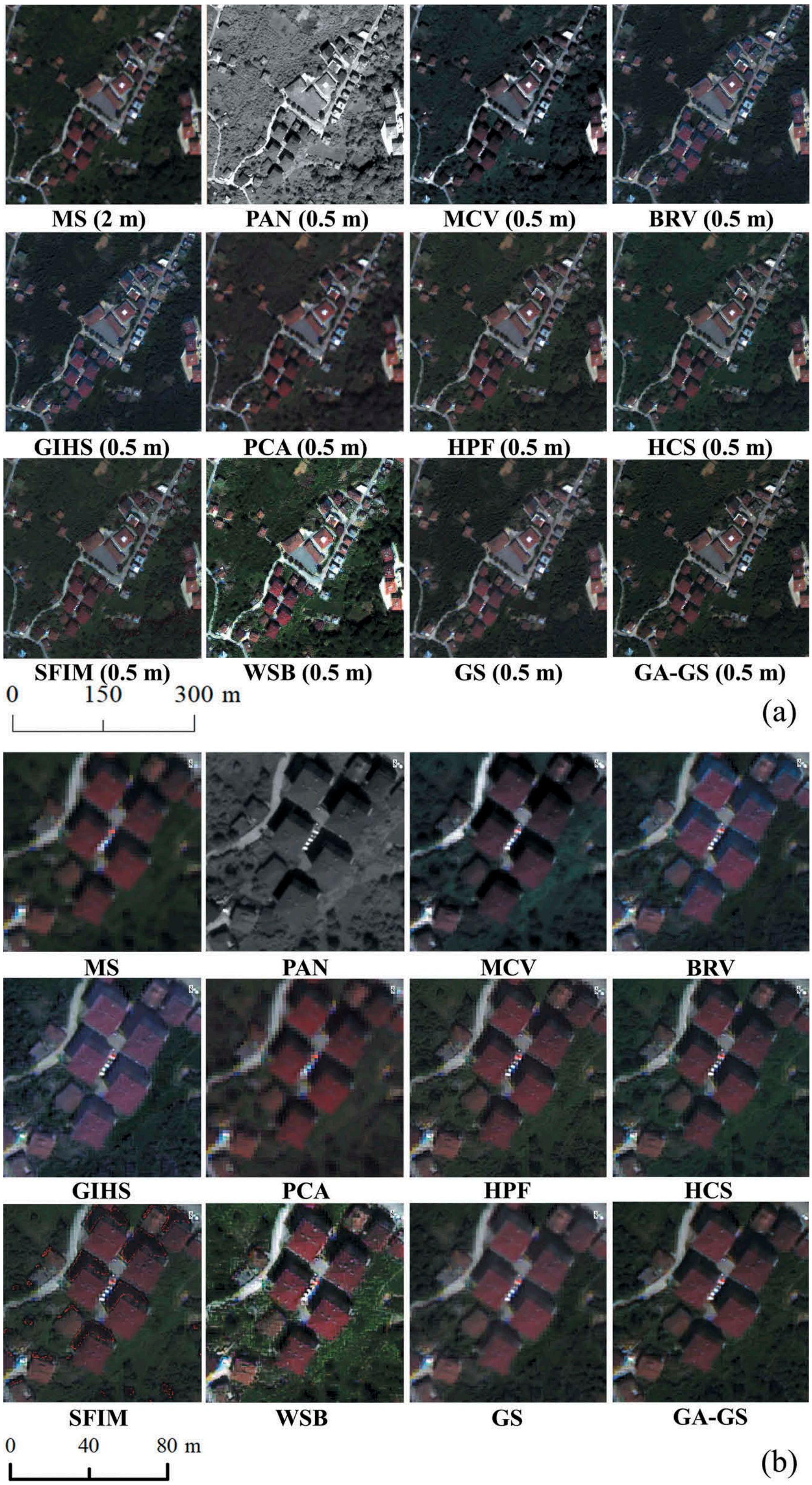

Figure 4. (a) Fused images for the site 2, (b) subsamples from (a).

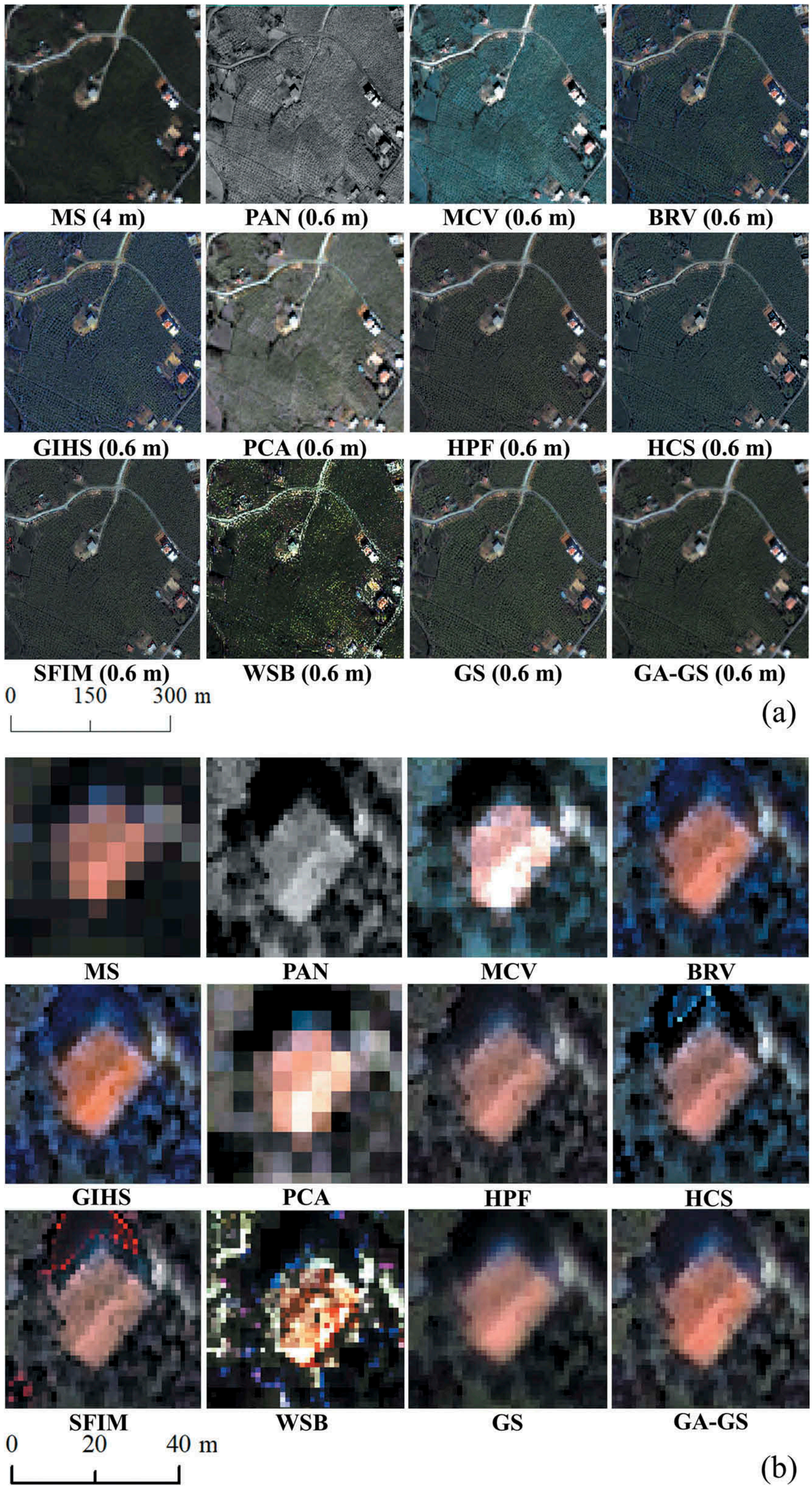

Figure 5. (a) Fused images for the site 3, (b) subsamples from (a).

Table 4. Spectral quality metric values calculated for the test sites (The best values are highlighted with grey).

Site	Method	Spectral quality metrics							
		RMSE	ERGAS	FSIM	UIQI	VIFF	FMI	GSM	SSIM
1	**MCV**	1003.214	17.796	0.004	0.000	0.840	0.860	0.000	0.000
	BRV	102.117	6.297	0.765	0.198	0.258	0.802	0.923	0.461
	GIHS	100.758	6.294	0.762	0.195	0.260	0.804	0.628	0.447
	PCA	89.534	3.806	0.819	0.272	0.338	0.859	0.944	0.608
	HPF	104.500	6.410	0.805	0.252	0.276	0.803	0.932	0.542
	HCS	132.299	8.399	0.737	0.193	0.308	0.794	0.643	0.444
	SFIM	105.236	6.538	0.802	0.253	0.278	0.800	0.933	0.548
	WSB	86.798	3.241	0.843	0.273	0.372	0.830	0.950	0.632
	GS	101.533	6.325	0.767	0.199	0.258	0.805	0.922	0.463
	GA-GS	73.249	2.741	0.844	0.365	0.495	0.858	0.954	0.676
2	**MCV**	984.255	31.497	0.005	0.000	0.101	0.910	0.000	0.000
	BRV	141.911	11.672	0.610	0.024	0.053	0.840	0.888	0.165
	GIHS	143.635	12.592	0.598	0.022	0.057	0.839	0.879	0.117
	PCA	347.568	15.007	0.795	0.284	0.231	0.873	0.788	0.469
	HPF	147.462	11.634	0.631	0.019	0.044	0.834	0.894	0.225
	HCS	146.771	11.595	0.623	0.020	0.046	0.833	0.892	0.191
	SFIM	194.912	27.098	0.627	0.019	0.045	0.846	0.889	0.231
	WSB	62.995	4.741	0.826	0.239	0.314	0.848	0.956	0.625
	GS	140.126	11.541	0.630	0.025	0.050	0.847	0.896	0.253
	GA-GS	46.317	3.131	0.846	0.363	0.455	0.891	0.965	0.699
3	**MCV**	763.320	16.079	0.002	0.000	1.663	0.880	0.023	0.000
	BRV	98.301	3.941	0.564	0.036	0.051	0.823	0.906	0.257
	GIHS	96.848	4.012	0.535	0.033	0.050	0.819	0.895	0.097
	PCA	242.627	9.782	0.013	0.018	0.050	0.871	0.243	0.111
	HPF	110.581	4.686	0.499	0.030	0.047	0.618	0.862	0.082
	HCS	119.629	5.056	0.466	0.025	0.052	0.826	0.843	0.072
	SFIM	134.225	7.179	0.496	0.027	0.047	0.835	0.857	0.084
	WSB	186.245	8.478	0.324	0.004	0.125	0.574	0.475	0.185
	GS	122.184	4.644	0.542	0.037	0.062	0.834	0.874	0.156
	GA-GS	59.467	3.001	0.881	0.455	0.429	0.897	0.912	0.530

was also justified by qualitative evaluation. Despite the fact that the MCV method produced an image with very low spectral fidelity in the site 1 (see Figure 3(a)), the VIFF and FMI metrics indicated the opposite. Of all methods, the MCV method got the best VIFF and FMI metric values in this site. This reveals the fact that the quality metrics may lead to misleading judgements about fusion outcomes. Hence, it is more reasonable to interpret the trend in multiple metric values, instead of judging fusion methods with a single quality metric.

Table 4 shows that the proposed GA-GS approach, again, got the best values for most of the metrics in the site 2. The GA-GS result got the best values from the RMSE, ERGAS, FSIM, UIQI, VIFF and GSM metrics. The MCV method was found to be the most successful one in terms of the FMI metric, whereas the SSIM metric indicated that the WSB yielded the optimum fusion result in the site 2. As seen from Table 4, the MCV, SFIM, GIHS and HCS methods did not manage to retain the colour features of the input MS image, whereas the HPF, BRV, PCA and GS methods preserved the colour characteristics to a small extent in the site 2.

Table 4 indicates that the GA-GS method achieved the best values from all spectral quality evaluation metrics in the site 3. The fused images produced by the BRV, GS and GIHS methods got promising spectral metric values in this site. On the other hand, the MCV, WSB and PCA methods got the worst spectral metric values in the site 3, which is also in compliance with visual findings (see Figure 5(a)). Although the BRV method seemed to change the global colour features in the site 3 (see Figure 5(a)), the metric values computed from the BRV fused image indicates the opposite, as this image got better metric values compared to the most of the other methods used. This attaches importance on considering the trend in multiple metric values to evaluate the colour quality of the fused images. It should also be kept in mind that there is no such thing as 'the best quality evaluation procedure' in the literature as each quality metric has its own mathematical theory, which leads to the fact that there may be inconsistencies among the values computed from different metrics. This is the main reason that almost all image fusion studies consider multiple metric values to evaluate the fusion results.

Table 5 presents the spectral quality scores given with respect to the methods' success in preserving the colour characteristics. Since a total of ten image fusion methods were used, each method got a score between 1 and 10. Since qualitative evaluation is a subjective task, visual findings were not scored. As seen from Table 5, the proposed GA-GS approach got the best average scores of 9.6, 9.9 and 10 in the sites 1, 2 and 3, respectively. The WSB method was found to be the second most successful one in the sites 1 and 2, whereas the BRV method got the second best average spectral quality score in the site 3. The PCA method was ranked as the third most successful one in the site 1, whereas the third most successful one in terms of colour fidelity in the sites 2 and 3 was the GS method. The worst average spectral quality score was obtained by the HCS

Table 5. Spectral quality scores given to fusion results in all test sites (The best values are highlighted with grey).

		Spectral quality score								
Site	Method	RMSE	ERGAS	FSIM	UIQI	VIFF	FMI	GSM	SSIM	Average
1	**MCV**	1	1	1	1	10	10	1	1	3.3
	BRV	5	6	4	4	2	3	5	4	4.1
	GIHS	7	7	3	3	3	5	2	3	4.1
	PCA	8	8	8	8	7	9	8	8	8.0
	HPF	4	4	7	6	4	4	6	6	5.1
	HCS	2	2	2	2	6	1	3	2	2.5
	SFIM	3	3	6	7	5	2	7	7	5.0
	WSB	9	9	9	9	8	7	9	9	8.6
	GS	6	5	5	5	1	6	4	5	4.6
	GA-GS	10	10	10	10	9	8	10	10	9.6
2	**MCV**	1	1	1	1	7	10	1	1	2.9
	BRV	7	5	3	6	5	4	4	3	4.6
	GIHS	6	4	2	5	6	3	3	2	3.9
	PCA	2	3	8	9	8	8	2	8	6.0
	HPF	4	6	7	2	1	2	7	5	4.3
	HCS	5	7	4	4	3	1	6	4	4.3
	SFIM	3	2	5	2	2	5	5	6	3.8
	WSB	9	9	9	8	9	7	9	9	8.6
	GS	8	8	6	7	4	6	8	7	6.8
	GA-GS	10	10	10	10	10	9	10	10	9.9
3	**MCV**	1	1	1	1	1	9	1	1	2.0
	BRV	8	9	9	8	6	4	9	9	7.8
	GIHS	9	8	7	7	5	3	8	5	6.5
	PCA	2	2	2	3	4	8	2	6	3.6
	HPF	7	6	6	6	3	2	6	3	4.9
	HCS	6	5	4	4	7	5	4	2	4.6
	SFIM	4	4	5	5	2	7	5	4	4.5
	WSB	3	3	3	2	9	1	3	8	4.0
	GS	5	7	8	9	8	6	7	7	7.1
	GA-GS	10	10	10	10	10	10	10	10	10.0

method in the site 1 and by the MCV method in the sites 2 and 3. Table 5 also reveals the fact that the GA-GS, GS, HCS, GIHS and BRV methods got the best average spectral quality score in the site 3, which is the most challenging site. The MCV, PCA and HPF methods achieved the best average spectral quality score in the site 1.

3.2.2. Spatial quality evaluation

Table 6 demonstrates the average CCs calculated between the fused bands and input PAN bands. Any fusion algorithms that increased the average CC with the input PAN image can be said to transfer the spatial details successfully. As seen from Table 6, all methods managed to increase the average CC in the site 1. The GA-GS method resulted in the greatest average CC increase (from 0.598 to 0.847) in the site 1. The PCA method followed the GA-GS method by a small margin in this site, increasing the average CC from 0.598 to 0.803. The average CC values given in Table 6 show that the WSB and MCV methods presented very similar performances in the site 1, which contradicts with visual findings. Table 6 also shows that the GS, GIHS and HCS methods yielded the smallest average CC increase in the site 1. Another conclusion drawn from Table 6 is that all methods except the SFIM and PCA managed to increase the average CC to some extent in the site 2. In this site, the GA-GS approach, again, achieved the greatest average CC increase (from 0.616 to 0.916). The MCV method provided the second greatest average CC increase (from 0.616 to 0.847) in the site 2. The HPF and BRV methods resulted in very similar average CC increase in this site. It can also be concluded from Table 6 that the HCS and WSB methods increased the average CC at the smallest extent in the site 2, whereas the SFIM and PCA methods decreased the average CC from 0.616 to 0.575 and to 0.366, respectively. The PCA and SFIM methods achieved a greater amount of average CC increase in the site 1, compared to the site 2. On the other hand, the GA-GS and MCV techniques yielded a greater amount of average CC increase in the site 2. Table 6 shows that all methods except the WSB managed to increase the average CC in the site 3. In this site, the GA-GS method was found to be the best one in transferring the spatial details. The GA-GS method increased the average CC from 0.311 to 0.817. As seen from Table 6, the second most successful one in terms of spatial fidelity was the GIHS method in the site 3. The GIHS method increased the average CC from 0.311 to 0.742. On the other hand, the BRV, HPF, GS, SFIM and HCS methods led to satisfying average CC increase in the site 3. It was also concluded that the PCA and MCV methods achieved the

Table 6. Average CCs and spatial quality scores for the test sites (The best values are highlighted with grey).

Method	Average CC site 1	Average CC site 2	Average CC site 3	Score site 1	Score site 2	Score site 3	Average score
MS/PAN	0.598	0.616	0.311	–	–	–	–
MCV/PAN	0.786	0.847	0.579	7	9	3	6.3
BRV/PAN	0.765	0.758	0.685	6	8	8	7.3
GIHS/PAN	0.675	0.713	0.742	2	6	9	5.7
PCA/PAN	0.803	0.366	0.348	9	1	2	4.0
HPF/PAN	0.747	0.750	0.679	5	7	7	6.3
HCS/PAN	0.668	0.676	0.642	1	4	4	3.0
SFIM/PAN	0.741	0.575	0.658	4	2	5	3.7
WSB/PAN	0.787	0.645	0.152	8	3	1	4.0
GS/PAN	0.697	0.703	0.674	3	5	6	4.7
GA-GS/PAN	0.847	0.916	0.817	10	10	10	10.0

smallest amount of average CC increase in this site. The WSB method failed to sharpen the input MS image of the site 3, as it decreased the average CC from 0.311 to 0.152.

The performance scores given with respect to the methods' spatial details transfer success are also given in Table 6. As seen from the table, the GA-GS approach was found to be the most successful one in increasing the spatial content in all test sites. It got the best average CC score of 10. The BRV and MCV methods were ranked as the second and third most successful ones in this regard, respectively. Table 6 also shows that the GIHS and HPF methods produced images with moderate spatial fidelity. On the other hand, the HCS, SFIM, GS, WSB and PCA methods got the smallest average CC scores. Figure 6 shows the average spectral and spatial quality scores to make it easier to interpret the scores given in Tables 5 and 6.

4. Discussion

This section discusses the working principles and performances of the image fusion methods used. The MCV technique simply multiplies each MS band with the PAN image to obtain the fused bands. This approach caused a significant amount of changes in the magnitude of the spectral vectors, causing colour distortions in both sites. This holds also true for the BRV method, which produces the fused images by multiplying each MS band with a constant defined by the ratio between the PAN and intensity band obtained by summing all MS bands.

The GIHS method eliminated the disadvantage of the conventional IHS method by processing more than three bands. However, it still suffers from producing images with low spectral fidelity, which was also pointed out by Ehlers et al. (2010). The performance of this method can be improved by changing or modifying the way the transformation between RGB and IHS spaces is done. Our observations revealed that matching the

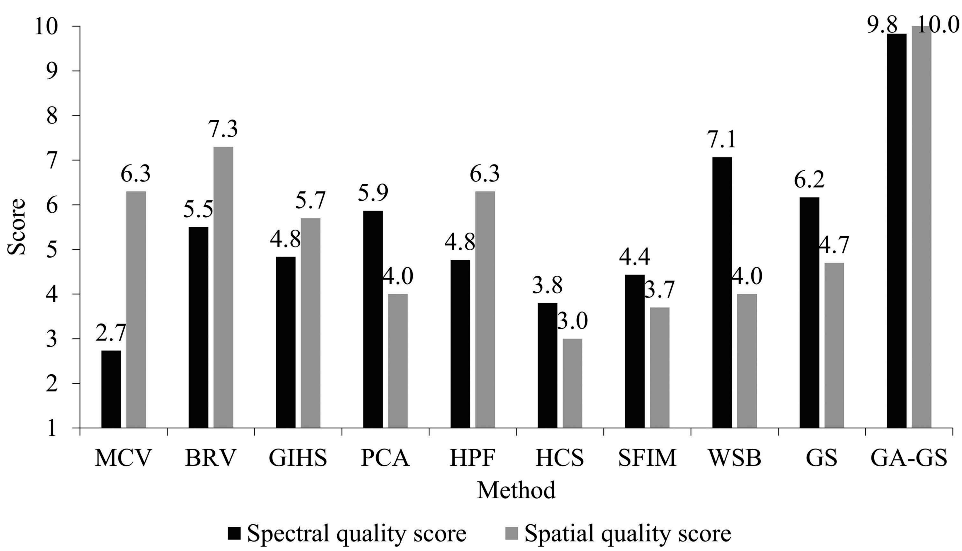

Figure 6. Average spectral and spatial quality scores.

histogram of the input PAN image to that of the intensity component prior to fusion allowed this method to keep the spectral content to some extent.

The performance of the PCA method depends heavily on the statistical characteristics of the input data used. If the input MS and PAN images have similar spectral characteristics, then the PCA method is likely to work well in spectral manner, as happened in this study. The reason for this is that, if the input MS and PAN images have statistically similar content, then the first principal component is likely to have a high correlation with the input PAN image, which will be replaced by the first principal component, preserving the colour content. As seen from Figure 6, the PCA method was ranked as the fourth (out of 10) most successful one in terms of spectral quality. Matching the histogram of the PAN image to that of the first principal component prior to fusion caused the absorption of a certain amount of the spatial content in the PAN image, which was the main reason that this method did not manage to transfer the spatial details properly, especially in the site 3.

The HPF method enhances the spatial details in the PAN image by employing a high-pass filter, which attaches importance to use an appropriate high-pass filter. The size and content of the filter have a direct effect on fusion performance. Unnecessarily larger-sized filters lead to unnecessarily sharper images, whereas smaller-sized filters affect the spatial detail transfer success. Smaller-sized filters help with the preservation of the colour characteristics, whereas larger-sized filters are likely to distort the colours. Hence, a compromise should be made between the filter size and fusion performance. The ERDAS IMAGINE software defines the size of the high-pass filter as a function of the spatial resolutions of the input MS and PAN images (ERDAS IMAGINE Field Guide). The ERDAS IMAGINE software also allows the users to perform a second high-pass filtering to further increase the spatial detail quality. However, in this study, we did not perform a second filtering, since the spatial resolution ratio between the input images were not high enough. In this study, the HPF method was found to manage to increase the spatial detail quality (see Figure 6). However, it was not that successful in keeping the colour content. The ERDAS IMAGINE software performs a linear stretch on the fused image to tackle this problem. However, we observed that performing a linear stretch increased the colour distortions to some extent. Instead, it is recommended to apply a histogram matching between the fused and input MS image to achieve higher spectral and spatial fidelity.

The HCS method produced fused images with low spectral and spatial quality. We believe that the spectral distortion caused by this method was due to the intensity scaling procedure. A more reasonable procedure may lead to spectrally and spatially more consistent images.

The SFIM method produces a smoothed PAN image by employing a mean filter on the input PAN image, which will then be divided by the smoothed PAN to obtain a constant to be multiplied by each MS band. Smoothing the PAN image this way did not only distort the colours but also led to the absorption of the spatial details, especially in the site 1. A different smoothing procedure (such as Gaussian) may yield images with high spectral and spatial fidelity.

The WSB method was found to keep the colour content in all test sites but the site 3. The method applies 2D DWT on the input PAN image to resolve it into its high and low frequency details. The main disadvantage of the 2D DWT is that it extracts high frequency details only in three directions (north-south, east-west and diagonal), which was the main reason for the spatial detail loss during subsequent DWTs.

The GS method is a statistical procedure like the PCA, which means that its result depends highly on its content. Matching the histogram of the first GS component to that of the PAN image enabled the preservation of the colours to some extent but caused spatial detail loss, as happened in the PCA procedure. On the other hand, the GS method simulated the low-resolution PAN image by averaging all MS bands, which was another cause for the spectral distortion. To eliminate this disadvantage and simulate a more effective low-resolution PAN image, the proposed GA-GS approach benefits from the GA to estimate a weight for each MS band. It enabled to transfer the spatial details with less colour distortion. The biggest advantage of the proposed approach is that it is very simple and does not rely on intense computations. It was concluded that the proposed GA-GS approach overcome the colour distortion disadvantage of the CS-based methods. Despite the fact that histogram matching between the GA-based low-resolution PAN band and input PAN band played an important role in keeping the colour balance, it caused a certain amount of spatial detail loss. This is understandable as we tried to achieve a balance between the spatial and spectral quality loss. The performance of the proposed approach can be improved by changing the population size, crossover rate and mutation rate parameters used by the GA. In this study, a crossover rate of 95% and a mutation rate of 1% were found to be efficient for the sites 1 and 3, whereas a crossover rate of 90% and a mutation rate of 0.3% were found to provide the optimum result in the site 2. On the other hand, a maximum iteration number of 100, 150 and 300 were found to be adequate for the sites 1, 2 and 3, respectively. Further increasing the population size and mutation rate may lead to spectrally more balanced images. However, increasing the population size will affect the computation time in a negative way.

5. Conclusion

This study proposed to modify the CS-based GS fusion method to improve its performance for producing more effective images to be used for image analysis. The modification was done by using the GA to estimate a weight for each MS band used to compute the low-resolution PAN image. The experiments revealed that the band weights of 0.24, 0.27, 0.24 and 0.24 gave the best RMSE in the site 1; the band weights of 0.05, 0.08, 0.15, 0.20, 0.21, 0.12, 0.11 and 0.07 yielded the optimum RMSE in the site 2; and the band weights of 0.18, 0.26, 0.19 and 0.38 achieved the best RMSE in the site 3. As seen from Figure 6, the proposed approach yielded spectrally and spatially superior results compared to the widely-used CS-based MCV, BRV, GIHS, PCA, HCS and GS methods. The GA-GS method also spectrally and spatially outperformed the MRA-based WSB method; and CB methods HPF and SFIM as well.

The GA has three major advantages: (1) It extensively samples the parameter space (Janssen, Ireland, and Ryckebusch 2003). This enables the proposed method to achieve the optimum band weights in a diverse search space. (2) It is not constrained by any assumptions relating to the search space such as continuity or existence of the derivatives (Adamiec et al. 2004). (3) It is easy to implement and does not rely on complex computations. These advantages make the GA appropriate for improving the performance of the GS fusion method. The use of GA in the GS method enables the estimation of the optimum band weights in a short span of time. However, choosing the appropriate population size parameter is challenging and often relies on trial-and-error, which may prolong the time to obtain the optimum solution. This parameter should be chosen

Table 7. Advantages and disadvantages/limitations of the GA-GS method.

Advantages	Disadvantages/Limitations
- Not dependent on the spatial resolution ratio between the input images - Not constrained by any assumptions - Able to search in a large parameter space - Easy to implement - Gives spectrally and spatially better results than the conventional GS method	- Hard to choose the appropriate population size parameter - Easy premature convergence

great enough to ensure the diversity of the population, otherwise, the obtained optimum band weights will not be the ones that are supposed to be. Another disadvantage of the GA is the ease of its premature convergence, which may affect the robustness of the optimum band weights found. Advantages and disadvantages/limitations of the proposed method are summarized in Table 7.

Image fusion is a good way of producing sharper images to be used for further analysis. Using the GA in fusion approaches enables the production of images of high spectral and spatial quality. Further studies will focus on using the GA to improve the performances of other fusion methods. We will also seek new strategies to increase the convergence speed of the proposed method.

Acknowledgements

We would like to thank the anonymous reviewers for their constructive comments and suggestions.

Disclosure statement

No potential conflict of interest was reported by the authors.

ORCID

Volkan Yilmaz http://orcid.org/0000-0003-0685-8369
Cigdem Serifoglu Yilmaz http://orcid.org/0000-0002-9738-5124
Oguz Güngör http://orcid.org/0000-0002-3280-5466
Jie Shan http://orcid.org/0000-0002-1948-9657

References

Adamiec, G., M. Garcia-Talavera, R. M. Bailey, and P. I. de La Torre. 2004. "Application of a Genetic Algorithm to Finding Parameter Values for Numerical Simulation of Quartz Luminescence." *Geochronometria: Journal on Methods & Applications of Absolute Chronology* 23 (9): 9–14.

Aiazzi, B., L. Alparone, S. Baronti, and A. Garzelli. 2002a. "Context-driven Fusion of High Spatial and Spectral Resolution Images Based on Oversampled Multiresolution Analysis." *IEEE Transactions on Geoscience and Remote Sensing* 40 (10): 2300–2312. doi:10.1109/TGRS.2002.803623.

Aiazzi, B., L. Alparone, S. Baronti, and M. Selva. 2002b. "Generalized Laplacian Pyramid-based Fusion of MS + P Image Data with Spectral Distortion Minimization." *ISPRS International Archives of Photogrammetry and Remote Sensing* 34 (3B–W3): 3–6.

Aiazzi, B., S. Baronti, and M. Selva. 2007. "Improving Component Substitution Pansharpening through Multivariate Regression of MS+Pan Data." *IEEE Transactions on Geoscience and Remote Sensing* 45 (10): 3230–3239. doi:10.1109/TGRS.2007.901007.

Alparone, L., B. Aiazzi, S. Baronti, and A. Garzelli. 2003. "Sharpening of Very High Resolution Images with Spectral Distortion Minimization." *Proceedings of the IEEE Geoscience and Remote Sensing Symposium (IGARSS'03)*, Toulouse, France, 1, 458–460. doi: 10.1109/IGARSS.2003.1293808.

Alparone, L., S. Baronti, A. Garzelli, and F. Nencini. 2004. "A Global Quality Measurement of Pan-sharpened Multispectral Imagery." *IEEE Geoscience and Remote Sensing Letters* 1 (4): 313–317. doi:10.1109/LGRS.2004.836784.

Cai, W., Y. Xu, Z. Wu, H. Liu, L. Qian, and Z. Wei. 2018. "Pan-Sharpening Based on Multilevel Coupled Deep Network." *IEEE International Geoscience and Remote Sensing Symposium (IGARSS)*, Valencia, Spain, pp. 7046–7049. doi: 10.1109/IGARSS.2018.8518121.

Chai, P., X. Luo, and Z. Zhang. 2017. "Image Fusion Using Quaternion Wavelet Transform and Multiple Features." *IEEE Access* 5: 6724–6734. doi:10.1109/ACCESS.2017.2685178.

Chavez, P. S., and A. Y. Kwarteng. 1989. "Extracting Spectral Contrast in Landsat Thematic Mapper Image Data Using Selective Principal Component Analysis." *Photogrammetric Engineering & Remote Sensing* 55 (3): 339–348.

Chen, L., X. Zhang, and H. Ma. 2018. "Sparse Representation over Shared Coefficients in Multispectral Pansharpening." *Tsinghua Science and Technology* 23 (3): 315–322. doi:10.26599/TST.2018.9010088.

Cheng, J., H. Liu, T. Liu, F. Wang, and H. Li. 2015. "Remote Sensing Image Fusion via Wavelet Transform and Sparse Representation." *ISPRS Journal of Photogrammetry and Remote Sensing* 104: 158–173. doi:10.1016/j.isprsjprs.2015.02.015.

Crippen, R. E. 1989. "A Simple Spatial Filtering Routine for the Cosmetic Removal of Scan-line Noise from Landsat TM P-tape Imagery." *Photogrammetric Engineering and Remote Sensing* 55: 327–331.

Dian, R., S. Li, L. Fang, and Q. Wei. 2019. "Multispectral and Hyperspectral Image Fusion with Spatial-spectral Sparse Representation." *Information Fusion* 49: 262–270. doi:10.1016/j.inffus.2018.11.012.

Dian, R., S. Li, A. Guo, and L. Fang. 2018. "Deep Hyperspectral Image Sharpening." *IEEE Transactions on Neural Networks and Learning Systems* 29: 5345–5355. doi:10.1109/TNNLS.2018.2798162.

Dong, L., Q. Yang, H. Wu, H. Xiao, and M. Xu. 2015. "High Quality Multi-spectral and Panchromatic Image Fusion Technologies Based on Curvelet Transform." *Neurocomputing* 159: 268–274. doi:10.1016/j.neucom.2015.01.050.

Ehlers, M., S. Klonus, P. Johan Åstrand, and P. Rosso. 2010. "Multi-sensor Image Fusion for Pansharpening in Remote Sensing." *Int. J. Image Data Fusion* 1 (1): 25–45. doi:10.1080/19479830903561985.

ERDAS IMAGINE v.13 Field Guide, Leica Geosystems. 2013.

Fei, R., J. Zhang, J. Liu, F. Du, P. Chang, and J. Hu. 2019. "Convolutional Sparse Representation of Injected Details for Pansharpening." *IEEE Geoscience and Remote Sensing Letters* 1–5. doi:10.1109/LGRS.2019.2904526.

Fernandez-Beltran, R., J. M. Haut, M. E. Paoletti, J. Plaza, A. Plaza, and F. Pla. 2018. "Remote Sensing Image Fusion Using Hierarchical Multimodal Probabilistic Latent Semantic Analysis." *IEEE Journal of Selected Topics in Applied Earth Observations and Remote Sensing* 11 (12): 4982–4993. doi:10.1109/JSTARS.2018.2881342.

Garzelli, A., and F. Nencini. 2006a. "Fusion of Panchromatic and Multispectral Images by Genetic Algorithms." *IEEE International Conference on Geoscience and Remote Sensing Symposium (IGARSS 2006)*, Denver, CO, USA, 3810–3813. doi: 10.1109/IGARSS.2006.976.

Garzelli, A., and F. Nencini. 2006b. "PAN-sharpening of Very High Resolution Multispectral Images Using Genetic Algorithms." *International Journal of Remote Sensing* 27 (15): 3273–3292. doi:10.1080/01431160600554991.

Garzelli, A., F. Nencini, and L. Capobianco. 2008. "Optimal MMSE Pan Sharpening of Very High Resolution Multispectral Images." *IEEE Transactions on Geoscience and Remote Sensing* 46 (1): 228–236. doi:10.1109/TGRS.2007.907604.

Ghahremani, M., and H. Ghassemian. 2015. "Remote-sensing Image Fusion Based on Curvelets and ICA." *International Journal of Remote Sensing* 36 (16): 4131–4143. doi:10.1080/01431161.2015.1071897.

Ghahremani, M., Y. Liu, P. Yuen, and A. Behera. 2019. "Remote Sensing Image Fusion via Compressive Sensing." *ISPRS Journal of Photogrammetry and Remote Sensing* 152: 34–48. doi:10.1016/j.isprsjprs.2019.04.001.

Ghassemian, H. 2016. "A Review of Remote Sensing Image Fusion Methods." *Information Fusion* 32: 75–89. doi:10.1016/j.inffus.2016.03.003.

Gogineni, R., and A. Chaturvedi. 2018. "Sparsity Inspired Pan-sharpening Technique Using Multiscale Learned Dictionary." *ISPRS Journal of Photogrammetry and Remote Sensing* 146: 360–372. doi:10.1016/j.isprsjprs.2018.10.009.

Haghighat, M. B. A., A. Aghagolzadeh, and H. Seyedarabi. 2011. "A Non-Reference Image Fusion Metric Based on Mutual Information of Image Features." *Computers & Electrical Engineering* 37 (5): 744–756. doi:10.1016/j.compeleceng.2011.07.012.

Hallada, W. A., and S. Cox. 1983. "Image Sharpening for Mixed Spatial and Spectral Resolution Satellite Systems." *Proceedings of the 17th International Symposium on Remote Sensing of Environment*, Ann Arbor, MI, 1023–1032.

Han, Y., Y. Cai, Y. Cao, and X. Xu. 2013. "A New Image Fusion Performance Metric Based on Visual Information Fidelity." *Information Fusion* 14 (2): 127–135. doi:10.1016/j.inffus.2011.08.002.

Hill, P., N. Canagarajah, and D. Bull. 2002. "Image Fusion Using Complex Wavelets." *Proceedings of the 13th British Machine Vision Conference*, Cardiff, UK, 487–496. doi: 10.5244/C.16.47.

Hole, K. R., V. S. Gulhane, and N. D. Shellokar. 2013. "Application of Genetic Algorithm for Image Enhancement and Segmentation." *International Journal of Advanced Research in Computer Engineering & Technology* 2 (4): 1342–1346.

Holland, H. 1975. *Adaptation in Natural and Artificial Systems*. Ann Arbor: University of Michigan Press.

Janssen, S., D. G. Ireland, and J. Ryckebusch. 2003. "Extraction of N* Information from the Limited P (γ, K+) Λ Data Set." *Physics Letters B* 562 (1–2): 51–56. doi:10.1016/S0370-2693(03)00557-4.

Khademi, G., and H. Ghassemian. 2017. "A Multi-objective Component-substitution-based Pansharpening." *3rd IEEE International Conference on Pattern Recognition and Image Analysis (IPRIA)*, Shahrekord, Iran, 248–252. doi: 10.1109/PRIA.2017.7983056.

Laben, C. A., and B. V. Brower. 2000. "Process for Enhancing the Spatial Resolution of Multispectral Imagery Using Pansharpening." US Patent No. 6,011,875, filed 29 April 1998 and issued 4 January 2000 to the Eastman Kodak Company.

Lam, Y. C., L. Y. Zhai, K. Tai, and S. C. Fok. 2004. "An Evolutionary Approach for Cooling System Optimization in Plastic Injection Moulding." *International Journal of Production Research* 42 (10): 2047–2061. doi:10.1080/00207540310001622412.

Lari, S. N., and M. Yazdi. 2016. "Improved IHS Pan-Sharpening Method Based on Adaptive Injection of À Trous Wavelet Decomposition." *International Journal of Signal Processing, Image Processing and Pattern Recognition* 9 (3): 291–308. doi:10.14257/ijsip.2016.9.3.26.

Li, S., X. Kang, and J. Hu. 2013. "Image Fusion with Guided Filtering." *IEEE Transactions on Image Processing* 22 (7): 2864–2875. doi:10.1109/TIP.2013.2244222.

Liu, A., W. Lin, and M. Narwaria. 2012. "Image Quality Assessment Based on Gradient Similarity." *IEEE Transactions on Image Processing* 21 (4): 1500–1512. doi:10.1109/TIP.2011.2175935.

Liu, J. G. 2000. "Smoothing Filter-based Intensity Modulation: A Spectral Preserve Image Fusion Technique for Improving Spatial Details." *International Journal of Remote Sensing* 21 (18): 3461–3472. doi:10.1080/014311600750037499.

Masi, G., D. Cozzolino, L. Verdoliva, and G. Scarpa. 2016. "Pansharpening by Convolutional Neural Networks." *Remote Sensing* 8 (7): 594. doi:10.3390/rs8070594.

Masoudi, R., and P. Kabiri. 2014. "New Intensity-hue-saturation Pan-sharpening Method Based on Texture Analysis and Genetic Algorithm-adaption." *Journal of Applied Remote Sensing* 8 (1): 083640. doi:10.1117/1.JRS.8.083640.

Maulik, U., and S. Bandyopadhyay. 2000. "Genetic Algorithm-based Clustering Technique." *Pattern Recognition* 33 (9): 1455–1465. doi:10.1016/S0031-3203(99)00137-5.

Maurer, T. 2013. “How to Pan-sharpen Images Using the Gram-Schmidt Pan-sharpen method—A Recipe.” *International Archives of the Photogrammetry, Remote Sensing and Spatial Information Sciences* XL-1/W1: 239–244. doi:10.5194/isprsarchives-XL-1-W1-239-2013.

Miao, Q. G., C. Shi, P. F. Xu, M. Yang, and Y. B. Shi. 2011. “A Novel Algorithm of Image Fusion Using Shearlets.” *Optics Communications* 284 (6): 1540–1547. doi:10.1016/j.optcom.2010.11.048.

Niazi, S. M. N., M. M. Zade, and F. S. Zadeh. 2016. “A Novel IHS-GA Fusion Method Based on Enhancement Vegetated Area.” *Journal of Geomatics Science and Technology* 6 (1): 235–248.

Otazu, X., M. González-Audícana, O. Fors, and J. Núñez. 2005. “Introduction of Sensor Spectral Response into Image Fusion Methods, Application to Wavelet-based Methods.” *IEEE Transactions on Geoscience and Remote Sensing* 43 (10): 2376–2385. doi:10.1109/TGRS.2005.856106.

Padwick, C., M. Deskevich, F. Pacifici, and S. Smallwood. 2010. “WorldView-2 Pansharpening.” *Proceedings of the ASPRS Annual Conference*, San Diego, CA, USA, 2630.

Palsson, F., J. R. Sveinsson, and M. O. Ulfarsson. 2017. “Multispectral and Hyperspectral Image Fusion Using a 3-d-convolutional Neural Network.” *IEEE Geoscience and Remote Sensing Letters* 14 (5): 639–643. doi:10.1109/LGRS.2017.2668299.

Park, J. H., and M. G. Kang. 2004. “Spatially Adaptive Multiresolution Multispectral Image Fusion.” *International Journal of Remote Sensing* 25 (23): 5491–5508. doi:10.1080/01431160412331270830.

Pohl, C., and J. van Genderen. 2016. *Remote Sensing Image Fusion: A Practical Guide*. Boca Raton, FL: CRC Press.

Qiu, M., Z. Ming, J. Li, K. Gai, and Z. Zong. 2015. “Phase-change Memory Optimization for Green Cloud with Genetic Algorithm.” *IEEE Transactions on Computers* 64 (12): 3528–3540. doi:10.1109/TC.2015.2409857.

Ranchin, T., B. Aiazzi, L. Alparone, S. Baronti, and L. Wald. 2003. “Image fusion—The ARSIS Concept and Some Successful Implementation Schemes.” *ISPRS Journal of Photogrammetry and Remote Sensing* 58 (1–2): 4–18. doi:10.1016/S0924-2716(03)00013-3.

Scarpa, G., S. Vitale, and D. Cozzolino. 2018. “Target-adaptive CNN-based Pansharpening.” *IEEE Transactions on Geoscience and Remote Sensing* 56 (9): 5443–5457. doi:10.1109/TGRS.2018.2817393.

Schowengerdt, R. A. 1980. “Reconstruction of Multispatial, Multispectral Image Data Using Spatial Frequency Content.” *Photogrammetric Engineering & Remote Sensing* 46 (10): 1325–1334.

Shao, Z., and J. Cai. 2018. “Remote Sensing Image Fusion with Deep Convolutional Neural Network.” *IEEE Journal of Selected Topics in Applied Earth Observations and Remote Sensing* 11 (5): 1656–1669. doi:10.1109/JSTARS.2018.2805923.

Shukla, A., H. M. Pandey, and D. Mehrotra. 2015. “Comparative Review of Selection Techniques in Genetic Algorithm.” *IEEE International Conference on Futuristic Trends on Computational Analysis and Knowledge Management*, Noida, India, pp. 515–519. doi:10.6026/97320630011515

Siddiqui, Y. 2003. “The Modified IHS Method for Fusing Satellite Imagery.” *Proceedings of the ASPRS Annual Conference*, Anchorage, Alaska, 5–9.

Singh, D., D. Garg, and H. Singh Pannu. 2017. “Efficient Landsat Image Fusion Using Fuzzy and Stationary Discrete Wavelet Transform.” *The Imaging Science Journal* 65 (2): 108–114. doi:10.1080/13682199.2017.1289629.

Singh, D., M. Kaur, and H. Singh. 2018. “Remote Sensing Image Fusion Using Fuzzy Logic and Gyrator Transform.” *Remote Sensing Letters* 9 (10): 942–951. doi:10.1080/2150704X.2018.1500044.

Snehmani, A. G., A. Ganju, S. Kumar, P. K. Srivastava, and H. Ram R P. 2017. “A Comparative Analysis of Pansharpening Techniques on QuickBird and WorldView-3 Images.” *Geocarto International* 32 (11): 1268–1284. doi:10.1080/10106049.2016.1206627.

Song, H., Q. Liu, G. Wang, R. Hang, and B. Huang. 2018. “Spatiotemporal Satellite Image Fusion Using Deep Convolutional Neural Networks.” *IEEE Journal of Selected Topics in Applied Earth Observations and Remote Sensing* 11 (3): 821–829. doi:10.1109/JSTARS.2018.2797894.

Tang, K. S., K. F. Man, S. Kwong, and Q. He. 1996. “Genetic Algorithms and Their Applications.” *IEEE Signal Processing Magazine* 13 (6): 22–37. doi:10.1109/79.543973.

Vargas, E., O. Espitia, H. Arguello, and J. Y. Tourneret. 2018. “Spectral Image Fusion from Compressive Measurements.” *IEEE Transactions on Image Processing* 28 (5): 2271–2282. doi:10.1109/TIP.2018.2884081.

Vicinanza, M. R., R. Restaino, G. Vivone, M. Dalla Mura, and J. Chanussot. 2014. "A Pansharpening Method Based on the Sparse Representation of Injected Details." *IEEE Geoscience and Remote Sensing Letters* 12 (1): 180–184. doi:10.1109/LGRS.2014.2331291.

Wald, L. 2002. "Data Fusion. Definitions and Architectures - Fusion of Images of Different Spatial Resolutions." In *Presses De l'Ecole*, 143-163. Ecole des Mines de Paris France.

Wald, L., and T. Ranchin. 2002. "Liu 'smoothing Filter-based Intensity Modulation: A Spectral Preserve Image Fusion Technique for Improving Spatial Details'." *International Journal of Remote Sensing* 23 (3): 593–597. doi:10.1080/01431160110088772.

Wald, L., T. Ranchin, and M. Mangolini. 1997. "Fusion of Satellite Images of Different Spatial Resolutions: Assessing the Quality of Resulting Images." *Photogrammetric Engineering and Remote Sensing* 63: 691–699.

Wang, W., L. Jiao, and S. Yang. 2014. "Fusion of Multispectral and Panchromatic Images via Sparse Representation and Local Autoregressive Model." *Information Fusion* 20: 73–87. doi:10.1016/j.inffus.2013.11.004.

Wang, X., S. Bai, Z. Li, R. Song, and J. Tao. 2019. "The PAN and MS Image Pansharpening Algorithm Based on Adaptive Neural Network and Sparse Representation in the NSST Domain." *IEEE Access* 7: 52508–52521. doi:10.1109/ACCESS.2019.2910656.

Wang, Z., and A. C. Bovik. 2002. "A Universal Image Quality Index." *IEEE Signal Processing Letters* 9 (3): 81–84. doi:10.1109/97.995823.

Wang, Z., and Q. Li. 2011. "Information Content Weighting for Perceptual Image Quality Assessment." *IEEE Transactions on Image Processing* 20 (5): 1185–1198. doi:10.1109/TIP.2010.2092435.

Wei, Q., J. Bioucas-Dias, N. Dobigeon, and J. Y. Tourneret. 2015. "Hyperspectral and Multispectral Image Fusion Based on a Sparse Representation." *IEEE Transactions on Geoscience and Remote Sensing* 53 (7): 3658–3668. doi:10.1109/TGRS.2014.2381272.

Wei, Q., J. Bioucas-Dias, N. Dobigeon, J. Y. Tourneret, M. Chen, and S. Godsill. 2016. "Multiband Image Fusion Based on Spectral Unmixing." *IEEE Transactions on Geoscience and Remote Sensing* 54 (12): 7236–7249. doi:10.1109/TGRS.2016.2598784.

Wei, Y., Q. Yuan, H. Shen, and L. Zhang. 2017. "Boosting the Accuracy of Multispectral Image Pansharpening by Learning a Deep Residual Network." *IEEE Geoscience and Remote Sensing Letters* 14 (10): 1795–1799. doi:10.1109/LGRS.2017.2736020.

Xing, Y., M. Wang, S. Yang, and L. Jiao. 2018. "Pan-sharpening via Deep Metric Learning." *ISPRS Journal of Photogrammetry and Remote Sensing* 145: 165–183. doi:10.1016/j.isprsjprs.2018.01.016.

Yang, B., and S. Li. 2012. "Pixel-level Image Fusion with Simultaneous Orthogonal Matching Pursuit." *Information Fusion* 13 (1): 10–19. doi:10.1016/j.inffus.2010.04.001.

Yang, J., Y. Q. Zhao, and J. C. W. Chan. 2018. "Hyperspectral and Multispectral Image Fusion via Deep Two-branches Convolutional Neural Network." *Remote Sensing* 10: 800. doi:10.3390/rs10050800.

Yang, Y., W. Wan, S. Huang, F. Yuan, S. Yang, and Y. Que. 2016. "Remote Sensing Image Fusion Based on Adaptive IHS and Multiscale Guided Filter." *IEEE Access* 4: 4573–4582. doi:10.1109/ACCESS.2016.2599403.

Yilmaz, V., and O. Gungor. 2016a. "Determining the Optimum Image Fusion Method for Better Interpretation of the Surface of the Earth." *Norsk Geografisk Tidsskrift-Norwegian Journal of Geography* 70 (2): 69–81. doi:10.1080/00291951.2015.1126761.

Yilmaz, V., and O. Gungor. 2016b. "Fusion of Very High-resolution UAV Images with Criteria-based Image Fusion Algorithm." *Arabian Journal of Geosciences* 9 (1): 59. doi:10.1007/s12517-015-2109-8.

Yilmaz, V., C. Serifoglu Yilmaz, and O. Gungor. 2019. "Genetic Algorithm-Based Synthetic Variable Ratio Image Fusion." *Geocarto International* (just-accepted), 1–17. doi:10.1080/10106049.2019.1629649.

Yin, H. 2015. "Sparse Representation Based Pansharpening with Details Injection Model." *Signal Processing* 113: 218–227. doi:10.1016/j.sigpro.2014.12.017.

Yin, H. 2019. "PAN-Guided Cross-Resolution Projection for Local Adaptive Sparse Representation-Based Pansharpening." *IEEE Transactions on Geoscience and Remote Sensing* 57 (7): 4938–4950. doi:10.1109/TGRS.2019.2894702.

Yu, M. 1998. "Image Segmentation Using Genetic Algorithm and Morphological Operations." Master Thesis, Iowa State University.

Yuan, Q., Y. Wei, X. Meng, H. Shen, and L. Zhang. 2018. "A Multiscale and Multidepth Convolutional Neural Network for Remote Sensing Imagery Pan-sharpening." *IEEE Journal of Selected Topics in Applied Earth Observations and Remote Sensing* 11 (3): 978–989. doi:10.1109/JSTARS.2018.2794888.

Zhang, K., M. Wang, and S. Yang. 2016. "Multispectral and Hyperspectral Image Fusion Based on Group Spectral Embedding and Low-rank Factorization." *IEEE Transactions on Geoscience and Remote Sensing* 55 (3): 1363–1371. doi:10.1109/TGRS.2016.2623626.

Zhang, L., L. Zhang, X. Mou, and D. Zhang. 2011. "FSIM: A Feature Similarity Index for Image Quality Assessment." *IEEE Transactions on Image Processing* 20 (8): 2378–2386. doi:10.1109/TIP.2011.2109730.

Zhang, Y. 1999. "A New Merging Method and Its Spectral and Spatial Effects." *International Journal of Remote Sensing* 20 (10): 2003–2014. doi:10.1080/014311699212317.

Zhao, W., H. Lu, and D. Wang. 2017. "Multisensor Image Fusion and Enhancement in Spectral Total Variation Domain." *IEEE Transactions on Multimedia* 20 (4): 866–879. doi:10.1109/TMM.2017.2760100.